

GS-ROR: 3D Gaussian Splatting for Reflective Object Relighting via SDF Priors

ZUO-LIANG ZHU, Nankai University, China
 BEIBEI WANG[†], Nanjing University, China
 JIAN YANG[†], Nankai University, China

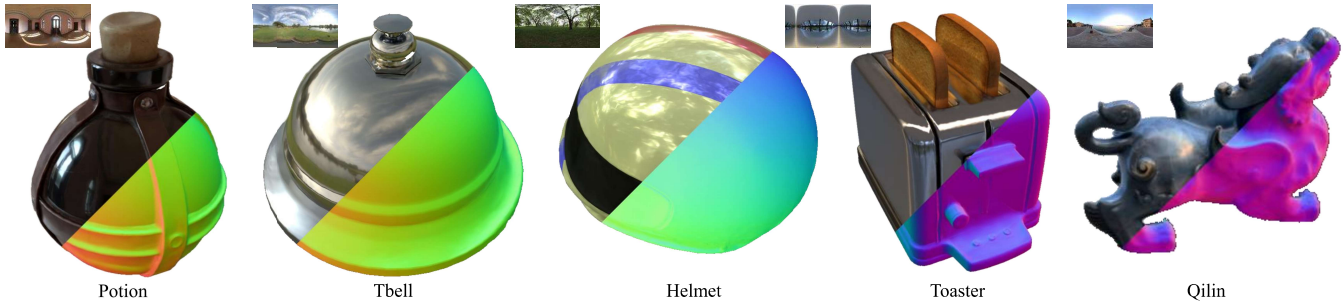


Fig. 1. We present an SDF-aided Gaussian Splatting framework for Reflective Object Relighting (GS-ROR) from multi-view images. We show five relighting results with reflective highlights (left) and their normal estimation (right), including POTION and TBELL from NeRO [Liu et al. 2023], HELMET and TOASTER from Ref-NeRF [Verbin et al. 2022], and QILIN from NeLLF++ [Zhang et al. 2023], where QILIN is from the real scene. Our method demonstrates a robust geometry reconstruction for reflective surfaces and faithful material decomposition, leading to photo-realistic and real-time reflective object relighting.

3D Gaussian Splatting (3DGS) has shown a powerful capability for novel view synthesis due to its detailed expressive ability and highly efficient rendering speed. Unfortunately, creating relightable 3D assets with 3DGS is still problematic, particularly for reflective objects, as its discontinuous representation raises difficulties in constraining geometries. Inspired by previous works, the signed distance field (SDF) can serve as an effective way for geometry regularization. However, a direct incorporation between Gaussians and SDF significantly slows training. To this end, we propose *GS-ROR* for reflective objects relighting with 3DGS aided by SDF priors. At the core of our method is the *mutual supervision* of the depth and normal between deferred Gaussians and SDF, which avoids the expensive volume rendering of SDF. Thanks to this mutual supervision, the learned deferred Gaussians are well-constrained with a minimal time cost. As the Gaussians are rendered in a deferred shading mode, while the alpha-blended Gaussians are smooth, individual Gaussians may still be outliers, yielding floater artifacts. Therefore, we further introduce an SDF-aware pruning strategy to remove Gaussian outliers, which are located distant from the surface defined by SDF, avoiding the floater issue. Consequently, our method outperforms the existing Gaussian-based inverse rendering methods in terms of relighting quality. Our method also exhibits competitive relighting quality compared to NeRF-based methods with at most 25% of training time and allows rendering at 200+ frames per second on an RTX4090.

CCS Concepts: • **Computing methodologies** → **Rendering**.

Additional Key Words and Phrases: neural rendering, Gaussian splatting, relighting

[†] Corresponding author.

Authors' addresses: Zuo-Liang Zhu, Nankai University, China, nkuzhuzl@gmail.com; Beibei Wang[†], Nanjing University, China, beibei.wang@nju.edu.cn; Jian Yang[†], Nankai University, China, csjyang@nankai.edu.cn.

1 INTRODUCTION

Creating relightable 3D assets from multi-view images has been a long-standing and challenging task in computer graphics and vision, as the decomposition of lighting, materials, and geometries is highly ill-posed. Particularly, the decomposition becomes more difficult for reflective objects, as their appearances are highly view-dependent, and a minor error on the surface leads to a significant difference. Existing approaches [Li et al. 2024; Liu et al. 2023] have shown impressive relighting quality for reflective objects by leveraging the neural radiance field (NeRF) and the signed distance field (SDF). Unfortunately, these methods require a long training and rendering time. In this paper, we aim at reflective objects relighting given multi-view images, simultaneously achieving high-quality relighting and short training/rendering time costs.

Most recently, Kerbl et al. [2023] proposed 3D Gaussian Splatting (3DGS), boosting the rendering speed significantly and achieving more detailed appearance modeling. A concurrent work [Ye et al. 2024] has introduced deferred Gaussian splatting for reflective objects, significantly improving the novel view synthesis (NVS) quality. Despite the impressive NVS quality, the relighting with 3DGS becomes problematic due to the Gaussians' discontinuity and high flexibility, especially for reflective objects. Extensive efforts have been made to improve the relighting quality by regularizing the geometry in terms of the normal and depth [Gao et al. 2023; Jiang et al. 2024; Liang et al. 2024]. However, they still suffer from erroneous surfaces and floater artifacts for reflective objects.

In this paper, we propose a novel framework *GS-ROR* for reflective objects relighting by leveraging SDF priors in the deferred Gaussian splatting. A direct incorporation between Gaussians and SDF significantly slows training, due to the expensive computational cost

of SDF rendering. For this, we propose to supervise the deferred Gaussians and SDF mutually in our framework, so-called *mutual-supervision*, which allows constraining deferred Gaussians with SDFs while avoiding SDF rendering. Specifically, the depth/normal of deferred Gaussians is supervised by SDF for regularization, while the SDF is supervised by Gaussians via the depth/normal rather than SDF rendering. This way, the learned deferred Gaussians are better constrained with a minimal computational cost. However, we still notice that Gaussians have floater artifacts occasionally, as the deferred Gaussians (with alpha blending) rather than individual Gaussians are constrained by SDF. Therefore, we introduce an SDF-aware pruning strategy to remove Gaussian outliers to avoid this floater issue. Consequently, our method outperforms the existing Gaussian-based inverse rendering methods in terms of relighting quality. Meanwhile, it exhibits competitive relighting quality compared to NeRF-based methods with at most 25% of training time. It also allows real-time rendering of reflective objects with 200+ frames per second on an RTX4090. To summarize, our main contributions include

- a GS-ROR framework for reflective object relighting, achieving high-quality relighting while maintaining short training time and allowing real-time rendering,
- a mutual supervision approach between deferred Gaussians and the SDF, producing robust geometry and avoiding local minima with minimal computational increase, and
- an SDF-aware Gaussian pruning strategy, which prunes outlier Gaussian, avoiding the float artifacts.

2 RELATED WORK

2.1 Neural representations for multi-view stereo

Since the presence of NeRF [Mildenhall et al. 2020], numerous neural implicit representations [Barron et al. 2022; Chen et al. 2022; Fridovich-Keil et al. 2022; Müller et al. 2022] have been proposed and gained remarkable progress in the field of multi-view stereo. These NeRF-based models adopt Multi-Layer Perceptrons (MLPs) [Barron et al. 2021, 2022; Verbin et al. 2022] or grid-like representations [Chen et al. 2022; Fridovich-Keil et al. 2022; Müller et al. 2022] to represent geometry and view-dependent appearance, optimized via volume rendering. Subsequently, NeuS [Wang et al. 2021] links the SDF with the density in NeRF and enables the optimization of surfaces with volume rendering. With extra regularization, these SDF-based models [Li et al. 2023; Rosu and Behnke 2023; Wang et al. 2023] achieve detailed surface reconstruction from RGB images. Owing to carefully designed architectures and specific optimization, some methods [Fridovich-Keil et al. 2022; Müller et al. 2022] enable fast training and real-time radiance field rendering.

3DGS [Kerbl et al. 2023] sheds light on the multi-view stereo in the rasterization framework, providing impressive real-time NVS results. 3DGS utilizes the discrete explicit 3D Gaussian primitive and projects these primitives onto the image plane to obtain the pixel color via alpha blending, which avoids the consuming sampling operation. However, 3DGS imposes no geometry constraint while optimizing, leading to noisy depth and normal, which hinders the usage of 3DGS in many downstream tasks. To resolve this issue,

existing methods construct different constraints on Gaussians by introducing 2D Gaussians [Huang et al. 2024] or Gaussian Surfel [Dai et al. 2024]. SuGaR [Guédon and Lepetit 2024] extracts a mesh from the Gaussians and binds the flattened Gaussians to the surface to optimize further. These methods improve the geometry quality significantly, which is orthogonal to our relighting framework and can further improve our relighting quality. We leave it for future work. NeuSG [Chen et al. 2023] introduces 3DGS into surface reconstruction to improve the details by optimizing NeuS and 3DGS jointly. Despite the high quality of the reconstructed surface, the training time is tens of times longer than 3DGS. Compared to their work, we also incorporate the SDF and Gaussians, but for different targets and in different ways, leading to a minimal time burden.

2.2 Inverse rendering

Inverse rendering aims to decompose geometry, material, and light from multi-view RGB images. Most existing methods adopt the geometry formulation from NeRF in either density or SDF manner, namely NeRF-based method. In terms of material modeling, most methods utilize the Disney Principled BRDF model [Burley and Studios 2012], while NeRFactor [Zhang et al. 2021b] pretrains a BRDF MLP with a measured BRDF dataset. Considering the light modeling, early works [Bi et al. 2020; Boss et al. 2021a,b; Zhang et al. 2022a, 2021a] consider direct light only, and more recent works [Jin et al. 2023; Srinivasan et al. 2021; Yang et al. 2023; Zhang et al. 2023, 2022b] model indirect lighting and visibility, leading to a higher-quality decomposition. However, these NeRF-based methods suffer from slow rendering speed and high training consumption.

More recently, Gaussian-based inverse rendering methods began to emerge. These methods regularize Gaussians to obtain a better geometry in diverse ways. Gaussian Shader [Jiang et al. 2024] and GIR [Shi et al. 2023] link the shortest axis of Gaussian with the normal. Gaussian Shader, Relightable Gaussian [Gao et al. 2023], and GS-IR [Liang et al. 2024] supervise the normal from Gaussian with the normal from the depth. To model the indirect illumination, Relightable Gaussian, GIR, and GS-IR compute the visibility via one-step ray tracing and represent the indirect illumination with SH coefficients. All these Gaussian-based relighting methods cannot relight reflective objects, while our method enables such scenarios.

2.3 Reflective objects NVS and relighting

As a special and challenging case, the NVS and relighting of reflective objects have drawn extensive attention. Ref-NeRF [Verbin et al. 2022] replaces the outgoing radiance with incoming radiance and models the shading explicitly with an integrated direction encoding (IDE) to improve the quality of reflective materials. MS-NeRF [Yin et al. 2023] designs a multi-space neural representation to model the reflection of mirror-like planes. Spec-NeRF [Ma et al. 2024] introduces a learnable Gaussian directional encoding to better model view-dependent effects. Spec-Gaussian [Yang et al. 2024] uses anisotropic spherical Gaussian to model view-dependent highlights. 3DGS-DR [Ye et al. 2024], as a concurrent work, introduces deferred shading into 3DGS. We also utilize a deferred framework, but for relighting, and together with other key components.

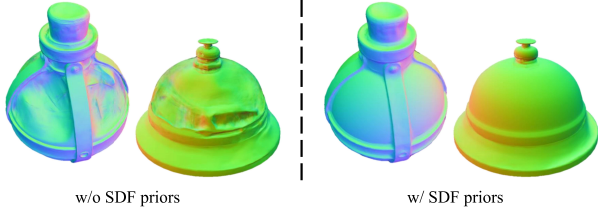


Fig. 2. The geometry from Gaussian is under-constrained and thus erroneous, while it is much better after utilizing the priors from the SDF.

Another group of methods enables relighting for reflective materials. NeRO [Liu et al. 2023] proposes a novel light representation consisting of two MLPs for direct and indirect light, respectively. With the explicit incorporation of the rendering equation, NeRO reconstructs reflective objects with high quality. TensoSDF [Li et al. 2024] designs roughness-aware incorporation between the radiance and reflectance field for robust geometry reconstruction and proposes a novel tensorial representation with SDF, enabling fast SDF query. Although their representation is faster than the original SDF, it still needs hours of training time and cannot achieve real-time rendering. Our method takes a further step in the reflective object relighting with 3D Gaussians and provides high-quality relighting results while keeping highly efficient training and rendering.

3 PRELIMINARIES AND MOTIVATION

In this section, we briefly review two ways for 3D scene representations and then discuss our motivation.

3D Gaussian Splatting. 3DGS represents a scene with a set of 3D Gaussians whose distribution is defined as

$$G(x) = e^{-\frac{1}{2}(x-\mu)^T \Sigma^{-1}(x-\mu)}, \quad (1)$$

where x is a position in the scene, μ is the mean of the Gaussian, and Σ denotes the covariance matrix of the 3D Gaussian, which is factorized into a scaling matrix S and a rotation matrix R as $\Sigma = RSS^T R^T$. To render an image, 3DGS projects the 3D Gaussians onto the image plane and employs alpha blending on the sorted 2D Gaussians as

$$C = \sum_{i \in \mathbb{N}} c_i \alpha_i \prod_{j=1}^{i-1} (1 - \alpha_j), \quad (2)$$

where c_i is the color of each Gaussian, and α_i is given by evaluating a projected 2D Gaussian with covariance Σ' multiplied with a learned per-point opacity.

SDF. An SDF expresses a scene by encoding the distance from the surface of an object, which can be expressed implicitly by an MLP [Wang et al. 2021] or in a hybrid way by combining a tensorial grid with a tiny MLP, called TensoSDF [Li et al. 2024], which allows more efficient training and rendering. Depth and normal are two significant attributes of geometry. In SDF, The point-wise depth D_j is defined as the distance from the camera to the sample, and the point-wise normal \mathbf{n}_j is commonly defined as the gradient of SDF ∇_x w.r.t. position x [Zhang et al. 2021a]. Given n points along the ray $p_i = \mathbf{o} + t\mathbf{v}$ where \mathbf{o} is the camera origin and \mathbf{v} is the view direction, we can aggregate these point-wise attributes to obtain

the attributes (*i.e.*, depth, normal) of the hit point of the surface as:

$$D_{\text{sdf}} = \sum_{i=0}^n w_i D_i, \quad \mathbf{n}_{\text{sdf}} = \sum_{i=0}^n w_i \mathbf{n}_i \quad (3)$$

where w_i is the weight of the i -th point derived from the SDF value.

SDF and NeRF can be unified by NeuS [Wang et al. 2021], which maps an SDF value to a density distribution. The distribution is defined as:

$$\phi_s(s) = \gamma e^{-\gamma s} / (1 + e^{-\gamma s})^2, \quad (4)$$

where s is the SDF value and γ is the inverse of standard deviation. Note that γ is a trainable parameter, and $1/\gamma$ approaches zero as the network training converges.

Motivation. The above two representations can both express a 3D scene, where the Gaussian representation is explicit and discontinuous, and the SDF is implicit (or hybrid) and continuous. These two representations lead to different rendering methods: splatting or rasterization for Gaussians and sphere tracing for SDF. While the Gaussian representation significantly boosts the rendering speed to a real-time level, it has difficulties constraining geometries, leading to inferior geometries, as shown in Fig. 2. A straightforward idea is to incorporate these two representations by leveraging the SDF as a prior. However, rendering SDF is time-consuming, which hinders the benefits of 3DGS. Therefore, the essential problem is an elegant incorporation between the Gaussians and the SDF.

4 METHOD

In this section, we present our framework GS-ROR for reflective object relighting. First, we present a deferred Gaussian splatting for relighting (Sec. 4.1). Then, we introduce the SDF priors into the deferred Gaussian splatting (Sec. 4.2) for geometry regularization. Finally, we propose an SDF-aware pruning strategy to refine the Gaussian distributions (Sec. 4.3).

4.1 Deferred Gaussian splatting for relighting

Starting from GS [Kerbl et al. 2023], we first construct a forward Gaussian splatting framework for relighting. Besides the radiance distribution represented with spherical harmonics (SH), each Gaussian also has reflectance parameters, defined by the Disney Principled BRDF model [Burley and Studios 2012]. The normal \mathbf{n} of Gaussian is defined as the combination of the shortest axis direction \mathbf{u} and an offset n_δ as $\mathbf{n} = \mathbf{u} + n_\delta$, following Gaussian Shader [Jiang et al. 2024]. The radiance from view \mathbf{v} for each Gaussian is computed by the split-sum approximation, following previous work [Jiang et al. 2024; Liang et al. 2024], and then aggregated by alpha blending. With multi-view images as inputs, the reflectance parameters at each Gaussian can be learned, besides the opacity and the environment map, enabling relighting under a novel environment map.

However, this simple Gaussian-based relighting baseline produces blurry relighting results for the reflective surface. The main reason behind this phenomenon is the alpha blending of Gaussians. As shown in Fig. 4, the Gaussians are overlapped to model an opaque surface with slightly different normals. While this difference among Gaussians causes a negligible error for rough objects, it amplifies the BRDF lobe for specular objects, leading to a blurry rendering.

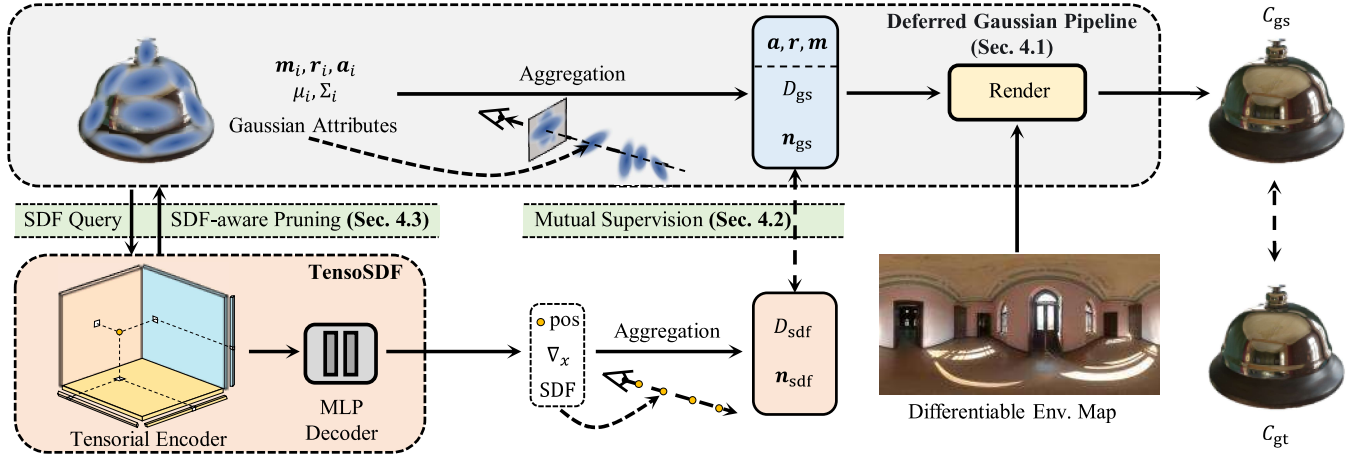


Fig. 3. Overview of our framework. The architecture of our proposed method consists of two geometry representations (*i.e.*, Gaussian primitive and TensoSDF). In the deferred Gaussian pipeline, the shading parameters (*i.e.*, albedo \mathbf{a} , roughness \mathbf{r} and metallicity \mathbf{m}), normal and depth are projected to the image plane and alpha blended. The pixel color C_{gs} is calculated using the split-sum approximation and supervised by ground truth color C_{gt} . In the TensoSDF, we sample rays originated from camera center \mathbf{o} and view direction \mathbf{v} and query the SDF value and gradient for each point p along the ray $\mathbf{o} + t\mathbf{v}$. The normal \mathbf{n}_{sdf} and depth D_{sdf} are obtained via volume rendering, which is supervised mutually with the normal \mathbf{n}_{gs} the depth D_{gs} from Gaussians. Note no color network is used in the SDF part, and only the geometry attributes are volume rendered.

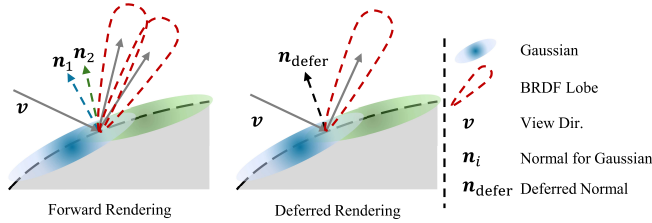


Fig. 4. Two Gaussians with a minor normal difference are overlapped to model an opaque surface. In the forward rendering, the BRDF values are computed w.r.t. to their own normal and are then alpha blended to form the final rendering, which is equivalent to a broader BRDF lobe, leading to a blurry rendering, eventually. In contrast, in the deferred shading, the BRDF is computed w.r.t. the deferred normal, maintaining the sharpness of reflective objects.

The key to addressing this issue is to blend the normals of Gaussians first and then perform shading, *i.e.*, deferred shading.

Specifically, we perform alpha blending on all the attributes (*e.g.*, normal, albedo, roughness) onto the image plane:

$$F = \sum_{i=0}^n f_i \alpha_i \prod_{j=1}^{i-1} (1 - \alpha_j), \quad (5)$$

where α_i, α_j share the same definition as in Eqn. (2), and f_i is a attribute of the i -th Gaussian. Then, we use split-sum approximation to compute the pixel-wise color.

The Gaussians are learned with the following loss function:

$$\mathcal{L}_{gs} = \mathcal{L}_c + \lambda_{nd} \mathcal{L}_{nd} + \lambda_{sm} \mathcal{L}_{sm} + \lambda_m \mathcal{L}_m + \lambda_{\delta n} \mathcal{L}_{\delta n}, \quad (6)$$

where \mathcal{L}_c is the color supervision between the rendered image and ground truth as in 3DGS, \mathcal{L}_{nd} is the supervision between the normal from Gaussian and from the estimated depth proposed in Gaussian Shader [Jiang et al. 2024], \mathcal{L}_{sm} is the smoothness loss for

BRDF parameters, \mathcal{L}_m is the mask loss, and $\mathcal{L}_{\delta n}$ is the delta normal regularization in Gaussian Shader. More details are shown in Sec. 5.

4.2 SDF-aided Gaussian splatting

Thanks to the deferred Gaussian splatting, the blurry issue for reflective object relighting has been addressed. However, the geometry established by Gaussians exhibits erroneous surfaces and floater artifacts, as it tends to overfit the appearance under the training light conditions. Hence, more constraints on the geometry are needed. Inspired by NeRO and TensoSDF, we introduce SDF into our framework, as it has shown to be a good prior for geometry regularization. The key is leveraging the capability of SDF while avoiding the expensive rendering. For this, we first choose a performance-friendly backbone for SDF – TensoSDF. Then, we propose a way of supervision between Gaussians and SDF, so-called *mutual supervision*, which avoids expensive SDF rendering.

TensoSDF. TensoSDF [Li et al. 2024] uses a tensorial representation for SDF, consisting of a tensorial encoder and MLP decoder, which is formulated as follows:

$$V_p = v_k^X \circ M_k^{YZ} \oplus v_k^Y \circ M_k^{XZ} \oplus v_k^Z \circ M_k^{XY}, s = \Theta(V_p, p), \quad (7)$$

where v_k^m and $M_k^{\bar{m}}$ represent the k -th vector and matrix factors of their corresponding spatial axes m , and \bar{m} denotes the two axes orthogonal to m *e.g.*, $\bar{X} = YZ$. \circ and \oplus represent the element-wise multiplication and concatenation operations. V_p is the latent vector from the tensorial encoder and then is decoded with the position p by a tiny MLP Θ to get the SDF value s . TensoSDF backbone enables a faster convergence speed and low-cost SDF query.

Mutual supervision. Even with a performance-friendly SDF backbone, the rendering of TensoSDF is still expensive, due to the required complex color network to represent the specular highlight

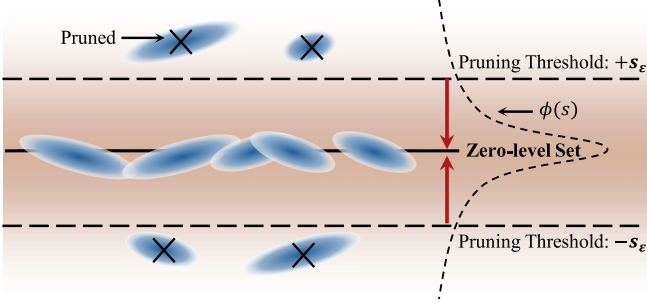


Fig. 5. The illustration of SDF-aware pruning. We define a narrowing threshold, which is adjusted automatically around the zero-level set. The Gaussians out of the threshold will be pruned. This pruning operation ensures all Gaussians are near the surface and avoids the floater artifact.

faithfully. Therefore, we propose to drop the SDF rendering and connect the SDF and Gaussians with geometry attributes.

Specifically, we pose supervision on the depth and normal of the SDF (Eqn. (3)) from Gaussians (Eqn. (2)):

$$\mathcal{L}_{gs2sdf} = |\mathbf{sg}[D_{gs}] - D_{sdf}| + (1 - \langle \mathbf{sg}[\mathbf{n}_{gs}], \mathbf{n}_{sdf} \rangle), \quad (8)$$

where D_{gs} and D_{sdf} are the depth from Gaussians and SDF, respectively, \mathbf{n}_{gs} and \mathbf{n}_{sdf} are normals from Gaussians and SDF respectively, and $\mathbf{sg}[\cdot]$ is the stop-gradient operation.

Besides the above loss, we also utilize the Eikonal loss \mathcal{L}_{eik} , Hessian loss \mathcal{L}_{hes} , mask loss \mathcal{L}_m , and total variance loss \mathcal{L}_{tv} to regularize the training of SDF, following common practice [Gropp et al. 2020; Li et al. 2024; Zhang et al. 2022c]. The final loss for SDF is

$$\mathcal{L}_{sdf} = \lambda_{gs2sdf} \mathcal{L}_{gs2sdf} + \lambda_{eik} \mathcal{L}_{eik} + \lambda_{hes} \mathcal{L}_{hes} + \mathcal{L}_m + \lambda_{tv} \mathcal{L}_{tv}, \quad (9)$$

where the $\lambda_{[\cdot]}$ is the corresponding coefficient to adjust the strength of regularization.

Then, we design another loss to update Gaussians with SDF priors:

$$\mathcal{L}_{sdf2gs} = |D_{gs} - \mathbf{sg}[D_{sdf}]| + (1 - \langle \mathbf{n}_{gs}, \mathbf{sg}[\mathbf{n}_{sdf}] \rangle). \quad (10)$$

Finally, we obtain the mutual supervision \mathcal{L}_{gs2sdf} and \mathcal{L}_{sdf2gs} , which bridges the SDF and Gaussian. Note that the stop-gradient operator is used to differ the strength of the supervisions of both sides.

4.3 SDF-aware pruning

With the deferred Gaussians supervised by SDF priors, the geometry becomes smoother. However, we still find noticeable floater artifacts, as no constraint is performed on individual Gaussian. To resolve this issue, we propose a Gaussian pruning strategy to enforce the Gaussians close to the zero-level set of SDF.

Specifically, for each Gaussian, we check the SDF value at its center and discard the Gaussian if the SDF value is larger than a threshold s_ϵ , as shown in the Fig. 5. Since it is laborious to adjust the threshold per scene, we link it with the probability density function $\phi_s(s)$ in Eqn. (4), which can be defined as:

$$s_\epsilon, \text{ where } \phi_s(s_\epsilon) = 0.01 (s_\epsilon > 0), \quad (11)$$

In this way, the threshold is determined automatically and narrowed with the SDF in the optimization, so we avoid posing a constant too strict when the surface is under-reconstructed and prune the Gaussians too far away from the surface in the end.

5 IMPLEMENTATION DETAILS

This section presents the network structures and the training details.

Network structures. The TensoSDF has a resolution of 400×400 with feature channels set as 36. The MLP decoder is a two-layer MLP whose width is 128. The Gaussian starts with 100K randomly initialized points.

Optimization details. The training of our framework includes three steps. Firstly, the deferred Gaussian splatting without any SDF supervision is trained separately for 1K iterations with Eqn. (6) to obtain a coarse geometry. Then, we freeze the Gaussians and warm up the TensoSDF via the depth and normal from Gaussians Eqn. (9) for 3K iterations. Finally, we train the entire framework with a joint loss for 24K iterations:

$$\mathcal{L}_{\text{joint}} = \mathcal{L}_{gs} + \lambda_{sdf2gs} \mathcal{L}_{sdf2gs}. \quad (12)$$

More details of the losses are in the supplementary material.

We train our model on an NVIDIA RTX 4090 and optimize it with Adam optimizer [Kingma and Ba 2014]. The learning rate for the TensoSDF [Li et al. 2024] grid and the MLP decoder is $1e^{-2}$ and $1e^{-3}$, respectively. The learning rate of Gaussian components follows the setting in 3DGS [Kerbl et al. 2023], and all attributes not in vanilla 3DGS have a learning rate of $2e^{-3}$. The initial resolution of TensoSDF is set to 128 and increases to the final resolution 400×400 , which uses only 60% capacity of the original TensoSDF, whose final resolution is 512×512 . After training, the TensoSDF will be discarded, and only Gaussians will be used for relighting. The optimization procedure takes about 1.5 hours in total.

6 RESULTS

In this section, we describe the evaluation setup (Sec. 6.1), and evaluate our relighting and NVS results (Sec. 6.2). Then, we conduct ablation studies on several main components (Sec. 6.2) and discuss limitations (Sec. 6.4).

6.1 Evaluation setup

Dataset. We evaluate our method on three synthetic datasets and one real-scene dataset. We utilize the TensoIR [Jin et al. 2023] synthetic and Glossy Blender dataset [Liu et al. 2023] to evaluate the performance of diffuse and specular materials, respectively. Besides, we use the Shiny Blender dataset to show the generalization ability of our method for diverse materials. For real scenes, we select some specular objects from the NeRF++ [Zhang et al. 2023].

Methods for comparison. We select 7 representative methods for comparison. We choose MII [Zhang et al. 2022b], TensoIR [Jin et al. 2023], TensoSDF [Li et al. 2024], and NeRO [Liu et al. 2023] for NeRF-based methods and Gaussian Shader [Jiang et al. 2024], GS-IR [Liang et al. 2024], and Relightable Gaussian [Gao et al. 2023] for Gaussian-based methods. We trained these models based on their public codes and configurations.

Metrics. We use the peak signal-to-noise ratio (PSNR) and structural similarity index (SSIM) [Wang et al. 2004] to measure the quality of results for the comparison and ablation study in the main paper. We present the learned perceptual image patch similarity

Table 1. Relighting quality in terms of PSNR \uparrow and SSIM \uparrow on the Blender Glossy dataset. Numbers in **bold** indicate the best performance, and underscored numbers indicate the second best. Although our method has higher numerical error than NeRO and TensoSDF, *the visual quality is comparable* (see Fig. 7).

	NeRF-based				Gaussian-based			
	MII	TensoIR	TensoSDF	NeRO	GShader	GS-IR	RelightGS	Ours
Angel	16.24/.8236	10.24/.2238	<u>20.40/.8969</u>	16.21/.7819	17.49/.8336	15.64/.6126	16.65/.8013	20.81/.8775
Bell	17.41/.8594	10.11/.1018	<u>29.91/.9767</u>	31.19/.9794	19.01/.8804	12.61/.2807	16.15/.8391	24.49/.9267
Cat	17.68/.8521	9.10/.1644	26.12/.9354	28.42/.9579	16.00/.8642	18.04/.7907	17.49/.8503	<u>26.28/.9421</u>
Horse	20.98/.8997	10.42/.1931	27.18/.9567	<u>25.56/.9437</u>	22.49/.9262	17.40/.7270	20.63/.8832	23.31/.9376
Luyu	17.89/.8050	8.27/.2375	19.91/.8825	26.22/.9092	15.62/.8254	19.00/.7727	17.47/.8168	<u>22.61/.8995</u>
Potion	17.13/.8094	6.21/.0846	<u>27.71/.9422</u>	30.14/.9561	12.33/.7575	16.37/.7051	14.99/.7799	25.67/.9175
Tbell	16.54/.8262	7.47/.1609	<u>23.33/.9404</u>	25.45/.9607	14.42/.8007	14.35/.5419	15.99/.7965	22.80/.9180
Teapot	16.71/.8546	9.96/.2093	<u>25.16/.9482</u>	29.87/.9755	18.21/.8560	16.63/.7646	17.36/.8389	21.17/.8932
Mean	17.57/.8413	8.97/.1719	<u>24.97/.9349</u>	26.63/.9331	16.95/.8430	16.26/.6494	17.09/.8258	23.39/.9140
Training Time	4h	5h	6h	12h	0.5h	0.5h	1h	1.5h
Ren. Time (FPS)	1/30	1/60	1/4	1/4	50	214	1.5	208

(LPIPS) [Zhang et al. 2018] in the supplementary materials. Due to the ambiguity between albedo and light, we normalize the relighting images to match the average colors of ground-truth images before computing the metrics, following NeRO. When the ground truth albedo is available, we rescale the relighting images based on the ground truth albedo and predicted albedo, following TensoIR. We record the mean training time and the frame per second (FPS)¹ in the evaluation, which tests on a single RTX 4090.

6.2 Comparison with previous works

Relighting of reflective objects. We evaluate the relighting performance of specular materials on the Glossy Blender dataset. The quantitative measurements are shown in Tab. 1, and the relighting visualizations are placed in Fig. 7. Our method outperforms other Gaussian-based methods and achieves competitive results of the NeRF-based methods. We also show the decomposed maps in Fig. 8 and Fig. 9. Due to the SDF priors and the deferred Gaussian pipeline, our method can produce a smooth surface without losing details and predict reasonable BRDF parameters.

Relighting of diffusion objects. Although our design focuses on reflective surfaces, it can also show benefits for diffuse objects. We validate our method on the TensoIR dataset. The quantitative measurements are shown in Tab. 2. The comparison with NeRF-based methods and relighting visualizations are in the supplementary material. Our methods can outperform the existing Gaussian-based methods and some NeRF-based methods on the TensoIR dataset, which reveals the robustness under diverse materials.

Relighting on real data. For real scenes, we select some objects with specular highlights from NeILF++ [Zhang et al. 2023], and the results are shown in Fig. 10. As there is no available ground truth, we only show the reference training views and some results under novel light conditions. Our method produces reasonable relighting results under novel lighting. Besides, our method achieves

¹NeRO and TensoSDF use the Cycles Render Engine in Blender to provide relighting results, so the FPS depends on samples per pixel, which is 1024 in our case.

Table 2. Relighting quality in terms of PSNR \uparrow and SSIM \uparrow on the TensoIR synthetic dataset. Numbers in **bold** indicate the best performance, and underscored numbers indicate the second best.

	GShader	GS-IR	RelightGS	Ours
Armad.	22.86/.9280	27.65/.9078	<u>30.76/.9526</u>	31.33/.9593
Ficus	24.61/.9491	23.63/.8662	27.23/.9637	<u>26.28/.9542</u>
Hotdog	17.45/.8838	21.51/.8853	<u>24.59/.9162</u>	25.21/.9307
Lego	13.41/.7904	<u>22.88/.8342</u>	22.49/.8682	25.46/.9083
Mean	19.58/.8878	23.92/.8734	<u>26.27/.9252</u>	27.07/.9381

Table 3. NVS quality in terms of PSNR \uparrow and SSIM \uparrow on the Glossy Blender dataset. Numbers in **bold** indicate the best performance, and underscored numbers indicate the second best.

	GS-IR	RelightGS	GShader	Ours
Angel	20.77/.6935	23.12/.7841	<u>27.14/.9226</u>	29.32/.9445
Bell	19.05/.4895	24.38/.8952	<u>30.00/.9409</u>	31.53/.9694
Cat	27.91/.9075	29.73/.9487	<u>31.25/.9604</u>	31.72/.9672
Horse	20.85/.6835	22.88/.7769	<u>26.03/.9314</u>	27.09/.9479
Luyu	24.96/.8637	25.97/.8986	<u>27.35/.9175</u>	28.53/.9383
Potion	25.81/.8217	29.03/.9277	<u>29.53/.9357</u>	30.51/.9503
Tbell	20.72/.6193	23.03/.8878	<u>23.86/.9031</u>	29.48/.9648
Teapot	20.56/.8427	20.82/.8719	23.56/.8986	26.41/.9468
Mean	22.58/.6322	24.87/.8739	<u>27.34/.9263</u>	29.32/.9537

a balance between quality and training speed, enabling reflective surface modeling with only 25% training time of TensoSDF and 13% of NeRO. Our method supports real-time rendering with 200+ FPS, much faster than all NeRF-based and some Gaussian-based methods.



Fig. 6. The comparison between the relighting results (above) and normal (below) of the variants starting from baseline.

NVS. We also present the NVS results on the Glossy Blender dataset. The quantitative evaluation in terms of PSNR and SSIM is present in Tab. 3. Our method can provide high-quality NVS results with sharper highlights, which are present in the supplementary materials, revealing the wide applications of our method.

6.3 Ablation study

We conduct ablation studies on the key components of our model on the Glossy Blender dataset. The mean relighting PSNR and SSIM are presented in the Tab. 5. We can see a consistent improvement when we employ new components to the model. We start from a baseline that first computes colors for Gaussians and alpha blends them as in 3DGS. As shown in the 1st column in Fig. 6, the baseline cannot render a reflective surface and provide the result with obvious artifacts due to the blending issue discussed in Sec. 4.1.

Deferred Gaussian pipeline. After applying the deferred Gaussian pipeline, this variant provides a more specular result. However, due to the erroneous normal, the surface reflects light from the wrong directions, shown in the 2nd column of Fig. 6.

TensoSDF incorporation. Then, we incorporate the TensoSDF and utilize its priors to regularize the geometry. The model without TensoSDF is vulnerable to the local minima and overfits under the training light condition, leading to erroneous geometry estimation. After employing the TensoSDF (3rd column in Fig. 6), the model mitigates the ambiguity between material and geometry and predicts a reasonable normal. We also validate the effectiveness of our mutual supervision by comparing it to supervision by a pretrained TensoSDF. As shown in Tab. 4, although using the pretrained TensoSDF for supervision could improve the quality slightly, it needs 5 hours for TensoSDF training. In contrast, our method achieves a balance between performance and efficiency.

SDF-aware pruning. Eventually, we apply the SDF-aware pruning operation to our model. The models without pruning are likely to overfit under training views, and we can observe some unnecessary Gaussians under test views, causing severe floater artifacts. After applying pruning, all Gaussians are located near the surface at

Table 4. Comparison of the relighting quality between mutual supervision (Ours) and using a pretrained TensoSDF to supervise Gaussians unidirectionally on the Glossy Blender dataset. Despite the slight improvement in quality, using the pretrained model leads to an extensive training time cost.

	Angel	Cat	Horse
Ours	20.81	26.28	23.31
Pretrained	21.45 (+0.64/+5h)	26.37 (+0.09/+5h)	24.59 (+1.28/+5h)

Table 5. Ablation study of three key components on the Glossy Blender dataset. “Def.” means the deferred Gaussian pipeline, “Inc.” means the incorporation of SDF and Gaussian, and “Pru.” means the pruning operation.

Components			Scene		
Def.	Inc.	Pru.	Horse	Cat	Angel
			20.33/0.9012	24.18/0.9253	18.86/0.8562
✓			20.59/0.9089	24.87/0.9323	18.86/0.8574
✓	✓		23.12/0.9357	26.22/0.9417	20.48/0.8793
✓	✓	✓	23.31/0.9376	26.28/0.9421	20.81/0.8775

the end of the training, and the model provides relighting results without floater artifacts, as shown in the 4th column in Fig. 6.

6.4 Discussion and limitations

Our model improves the relighting quality compared to other Gaussian-based methods. However, some issues remain to be solved. The SDF representation used in our framework is used as a prior, and it can not be used for exporting a faithful mesh due to its low resolution. Besides, we observe the split-sum approximation in DiffRast [Laine et al. 2020] causes blurry renderings when the roughness is very small. Please see the supplementary materials. We believe replacing it with a more accurate rendering method will improve the relighting quality. Last, we only consider direct lighting in our framework, and introducing indirect illumination will benefit the relighting quality, and we leave it for future work.

7 CONCLUSION

In this paper, we present a novel framework for real-time reflective object inverse rendering. We design an SDF-aided Gaussian splatting framework, using the mutual supervision of the depth and normal between deferred Gaussians and SDF to improve the quality of geometry from Gaussians. Besides, we propose an SDF-aware pruning strategy with an automatically adjusted threshold, regularizing the position of Gaussian and avoiding the floater artifact. Consequently, our method outperforms the existing Gaussian-based inverse rendering methods without losing efficiency. It is competitive with the NeRF-based methods in terms of quality, with much less training and rendering time. In future work, extending our framework to complex scenarios with multiples objects is a potential direction.

REFERENCES

- Jonathan T. Barron, Ben Mildenhall, Matthew Tancik, Peter Hedman, Ricardo Martin-Brualla, and Pratul P. Srinivasan. 2021. Mip-NeRF: A Multiscale Representation for Anti-Aliasing Neural Radiance Fields. In *ICCV*.
- Jonathan T. Barron, Ben Mildenhall, Dor Verbin, Pratul P. Srinivasan, and Peter Hedman. 2022. Mip-NeRF 360: Unbounded Anti-Aliased Neural Radiance Fields. In *CVPR*.
- Sai Bi, Zexiang Xu, Pratul Srinivasan, Ben Mildenhall, Kalyan Sunkavalli, Miloš Hašan, Yannick Hold-Geoffroy, David Kriegman, and Ravi Ramamoorthi. 2020. Neural Reflectance Fields for Appearance Acquisition. *ACM TOG* (2020).
- Mark Boss, Raphael Braun, Varun Jampani, Jonathan T. Barron, Ce Liu, and Hendrik P.A. Lensch. 2021a. NeRD: Neural Reflectance Decomposition from Image Collections. In *ICCV*.
- Mark Boss, Varun Jampani, Raphael Braun, Ce Liu, Jonathan T. Barron, and Hendrik P.A. Lensch. 2021b. Neural-PIL: Neural Pre-Integrated Lighting for Reflectance Decomposition. In *NeurIPS*.
- Brent Burley and Walt Disney Animation Studios. 2012. Physically-based shading at disney. In *SIGGRAPH*.
- Anpei Chen, Zexiang Xu, Andreas Geiger, Jingyi Yu, and Hao Su. 2022. TensorRF: Tensorial Radiance Fields. In *ECCV*.
- Hanlin Chen, Chen Li, and Gim Hee Lee. 2023. NeuSG: Neural Implicit Surface Reconstruction with 3D Gaussian Splatting Guidance. (2023). arXiv:2312.00846
- Pinxuan Dai, Jiamin Xu, Wenxiang Xie, Xinguo Liu, Huamin Wang, and Weiwei Xu. 2024. High-quality Surface Reconstruction using Gaussian Surfels. In *SIGGRAPH*.
- Sara Fridovich-Keil, Alex Yu, Matthew Tancik, Qinhong Chen, Benjamin Recht, and Angjoo Kanazawa. 2022. Plenoxels: Radiance fields without neural networks. In *CVPR*.
- Jian Gao, Chun Gu, Youtian Lin, Hao Zhu, Xun Cao, Li Zhang, and Yao Yao. 2023. Relightable 3D Gaussian: Real-time Point Cloud Relighting with BRDF Decomposition and Ray Tracing. (2023). arXiv:2311.16043
- Amos Gropp, Lior Yariv, Niv Haim, Matan Atzmon, and Yaron Lipman. 2020. Implicit Geometric Regularization for Learning Shapes. In *ICML*.
- Antoine Guédon and Vincent Lepetit. 2024. SuGaR: Surface-Aligned Gaussian Splatting for Efficient 3D Mesh Reconstruction and High-Quality Mesh Rendering. In *CVPR*.
- Binbin Huang, Zehao Yu, Anpei Chen, Andreas Geiger, and Shenghua Gao. 2024. 2DGS: 2D Gaussian Splatting for Geometrically Accurate Radiance Fields. *ACM TOG* (2024).
- Yingwenqi Jiang, Jiadong Tu, Yuan Liu, Xifeng Gao, Xiaoxiao Long, Wenping Wang, and Yuexin Ma. 2024. GaussianShader: 3D Gaussian Splatting with Shading Functions for Reflective Surfaces. In *CVPR*.
- Haian Jin, Isabella Liu, Peijia Xu, Xiaoshuai Zhang, Songfang Han, Sai Bi, Xiaowei Zhou, Zexiang Xu, and Hao Su. 2023. TensorIR: Tensorial Inverse Rendering. In *CVPR*.
- Bernhard Kerbl, Georgios Kopanas, Thomas Leimkühler, and George Drettakis. 2023. 3D Gaussian Splatting for Real-Time Radiance Field Rendering. *ACM TOG* (2023).
- Diederik P Kingma and Jimmy Ba. 2014. Adam: A method for stochastic optimization. (2014). arXiv:2312.05133
- Samuli Laine, Janne Hellsten, Tero Karras, Yeongho Seol, Jaakko Lehtinen, and Timo Aila. 2020. Modular Primitives for High-Performance Differentiable Rendering. *ACM TOG* (2020).
- Jia Li, Lu Wang, Lei Zhang, and Beibei Wang. 2024. TensorSDF: Roughness-aware Tensorial Representation for Robust Geometry and Material Reconstruction. In *SIGGRAPH*.
- Zhaoshuo Li, Thomas Müller, Alex Evans, Russell H Taylor, Mathias Unberath, Ming-Yu Liu, and Chen-Hsuan Lin. 2023. Neuralangelo: High-Fidelity Neural Surface Reconstruction. In *CVPR*.
- Zhihao Liang, Qi Zhang, Ying Feng, Ying Shan, and Kui Jia. 2024. Gs-ir: 3d gaussian splatting for inverse rendering. In *CVPR*.
- Yuan Liu, Peng Wang, Cheng Lin, Xiaoxiao Long, Jiepeng Wang, Lingjie Liu, Taku Komura, and Wenping Wang. 2023. NeRO: Neural Geometry and BRDF Reconstruction of Reflective Objects from Multiview Images. In *SIGGRAPH*.
- Li Ma, Vasu Agrawal, Haithem Turki, Changil Kim, Chen Gao, Pedro Sander, Michael Zollhöfer, and Christian Richardt. 2024. SpecNeRF: Gaussian Directional Encoding for Specular Reflections. arXiv:2312.13102
- Ben Mildenhall, Pratul P. Srinivasan, Matthew Tancik, Jonathan T. Barron, Ravi Ramamoorthi, and Ren Ng. 2020. NeRF: Representing Scenes as Neural Radiance Fields for View Synthesis. In *ECCV*.
- Thomas Müller, Alex Evans, Christoph Schied, and Alexander Keller. 2022. Instant Neural Graphics Primitives with a Multiresolution Hash Encoding. *ACM TOG* (2022).
- Radu Alexandru Rosu and Sven Behnke. 2023. PermutoSDF: Fast Multi-View Reconstruction with Implicit Surfaces using Permutohedral Lattices. In *CVPR*.
- Yahao Shi, Yanmin Wu, Chenming Wu, Xing Liu, Chen Zhao, Haocheng Feng, Jingtuo Liu, Liangjun Zhang, Jian Zhang, Bin Zhou, Errui Ding, and Jingdong Wang. 2023. GIR: 3D Gaussian Inverse Rendering for Relightable Scene Factorization. (2023). arXiv:2312.05133
- Pratul P Srinivasan, Boyang Deng, Xiuming Zhang, Matthew Tancik, Ben Mildenhall, and Jonathan T Barron. 2021. Nerv: Neural reflectance and visibility fields for relighting and view synthesis. In *CVPR*.
- Dor Verbin, Peter Hedman, Ben Mildenhall, Todd Zickler, Jonathan T. Barron, and Pratul P. Srinivasan. 2022. Ref-NeRF: Structured View-Dependent Appearance for Neural Radiance Fields. In *CVPR*.
- Peng Wang, Lingjie Liu, Yuan Liu, Christian Theobalt, Taku Komura, and Wenping Wang. 2021. NeuS: Learning Neural Implicit Surfaces by Volume Rendering for Multi-view Reconstruction. In *NeurIPS*.
- Zhou Wang, Alan C Bovik, Hamid R Sheikh, and Eero P Simoncelli. 2004. Image quality assessment: from error visibility to structural similarity. *IEEE TIP* (2004).
- Zixiong Wang, Yunxiao Zhang, Rui Xu, Fan Zhang, Pengshuai Wang, Shuangmin Chen, Shiqing Xin, Wenping Wang, and Changhe Tu. 2023. Neural-Singular-Hessian: Implicit Neural Representation of Unoriented Point Clouds by Enforcing Singular Hessian. *ACM TOG* (2023).
- Ziyi Yang, Yanzhen Chen, Xinyu Gao, Yazhen Yuan, Yu Wu, Xiaowei Zhou, and Xiaogang Jin. 2023. SIRE-IR: Inverse Rendering for BRDF Reconstruction with Shadow and Illumination Removal in High-Illuminance Scenes. arXiv:2310.13030
- Ziyi Yang, Xinyu Gao, Yangtian Sun, Yihua Huang, Xiaoyang Lyu, Wen Zhou, Shaohui Jiao, Xiaojuan Qi, and Xiaogang Jin. 2024. Spec-Gaussian: Anisotropic View-Dependent Appearance for 3D Gaussian Splatting. In *CVPR*.
- Keyang Ye, Qiming Hou, and Kun Zhou. 2024. 3D Gaussian Splatting with Deferred Reflection. In *SIGGRAPH*.
- Ze-Xin Yin, Jiaxiang Qiu, Ming-Ming Cheng, and Bo Ren. 2023. Multi-Space Neural Radiance Fields. In *CVPR*.
- Jingyang Zhang, Yao Yao, Shiwei Li, Tian Fang, David McKinnon, Yanghai Tsin, and Long Quan. 2022c. Critical regularizations for neural surface reconstruction in the wild. In *CVPR*.
- Jingyang Zhang, Yao Yao, Shiwei Li, Jingbo Liu, Tian Fang, David McKinnon, Yanghai Tsin, and Long Quan. 2023. NeLLF++: Inter-reflectable Light Fields for Geometry and Material Estimation. In *ICCV*.
- Kai Zhang, Fujun Luan, Zhengqi Li, and Noah Snavely. 2022a. IRON: Inverse Rendering by Optimizing Neural SDFs and Materials from Photometric Images. In *CVPR*.
- Kai Zhang, Fujun Luan, Qianqian Wang, Kavita Bala, and Noah Snavely. 2021a. PhysSG: Inverse Rendering with Spherical Gaussians for Physics-based Material Editing and Relighting. In *CVPR*.
- Richard Zhang, Phillip Isola, Alexei A Efros, Eli Shechtman, and Oliver Wang. 2018. The unreasonable effectiveness of deep features as a perceptual metric. In *CVPR*.
- Xiuming Zhang, Pratul P Srinivasan, Boyang Deng, Paul Debevec, William T Freeman, and Jonathan T Barron. 2021b. Nerfactor: Neural factorization of shape and reflectance under an unknown illumination. *ACM TOG* (2021).
- Yuanqing Zhang, Jiaming Sun, Xingyi He, Huan Fu, Rongfei Jia, and Xiaowei Zhou. 2022b. Modeling Indirect Illumination for Inverse Rendering. In *CVPR*.

Supplementary Material – GS-ROR: 3D Gaussian Splatting for Reflective Object Relighting via SDF Priors

1 LOSS DETAILS

We introduce the definition and weights of losses we used in the main paper. The color loss is defined as in 3DGS [Kerbl et al. 2023]

$$L_c = \lambda \|C_{gs} - C_{gt}\|_1 + (1 - \lambda)(1 - \text{SSIM}(C_{gs}, C_{gt})), \quad (1)$$

where C_{gs} is the rendered color from Gaussians and C_{gt} is the ground truth color. The coefficient λ is set to 0.8. The supervision L_{nd} from normal is defined as

$$L_{nd} = \|\hat{\mathbf{n}} - \mathbf{n}\|^2, \quad (2)$$

where $\hat{\mathbf{n}}$, \mathbf{n} are the normal from depth and the normal from Gaussians, respectively. Our normal formulation follows Gaussian Shader, which combines the shortest axis and a learnable residual [Jiang et al. 2024] as

$$\mathbf{n} = u + n_\delta, \quad (3)$$

where u is the shortest axis and n_δ is the residual term. To prevent the residual from dominating the normal direction, we add a penalty to it:

$$L_{\delta_n} = \|n_\delta\|^2. \quad (4)$$

The smoothness loss for BRDF parameters (*i.e.*, albedo \mathbf{a} , roughness \mathbf{r} , metallicity \mathbf{m}) is defined as

$$L_{sm} = \|\nabla f\| \exp^{-\|\nabla C_{gt}\|}, (f \in \{\mathbf{a}, \mathbf{r}, \mathbf{m}\}) \quad (5)$$

where ∇ is the gradient operator and C_{gt} is the color of ground-truth image. The mask loss is the binary cross entropy between predicted and ground-truth masks.

In the first phase, we set the corresponding weights $\lambda_{[\cdot]}$ as $\lambda_{nd} = 0.2$, $\lambda_{sm} = 1e^{-2}$, $\lambda_m = 0.2$, $\lambda_{\delta n} = 1e^{-3}$. In the second phase, the loss weights are set as $\lambda_{gs2sdf} = 0.5$, $\lambda_{eik} = 0.1$, $\lambda_{hes} = 5e^{-4}$, $\lambda_{tv} = 0.1$. In third phase, the loss weights are set as $\lambda_{sdf2gs} = 0.25$.

2 SPLIT-SUM APPROXIMATION

A typical rendering equation needs to compute an integral on the upper hemisphere involving incident light, view direction, normal, and BRDF (Bidirectional Reflectance Distribution Function):

$$c(\omega_o) = \int_{\Omega} L_i(\omega_i) f(\omega_i, \omega_o) (\omega_i \cdot \mathbf{n}) d\omega_i, \quad (6)$$

where $L_i(\omega_i)$ denotes the light from incident direction ω_i , $f(\omega_i, \omega_o)$ is the BRDF with respect to the incident direction ω_i and outgoing direction ω_o , and \mathbf{n} denotes the surface normal. In practice, the Disney Principled BRDF [Burley and Studios 2012] is the most widely used BRDF, consisting of a diffuse lobe and a specular lobe

$$f(\omega_i, \omega_o) = \underbrace{(1 - \mathbf{m}) \frac{\mathbf{a}}{\pi}}_{\text{diffuse}} + \underbrace{\frac{DFG}{4(\omega_i \cdot \mathbf{n})(\omega_o \cdot \mathbf{n})}}_{\text{specular}}, \quad (7)$$

where D is the normal distribution function, F is the Fresnel term, G is the geometry term, \mathbf{a} is the albedo, and \mathbf{m} is the metallicity. However, the integral is expensive to evaluate, and the split-sum

Author’s address:



Fig. 1. The comparison between the result using Cycle path-tracing renderer in Blender and the one using split-sum approximation in DiffRast. The split-sum result is blurry when the roughness of the surface is very small.

technique [Karis and Games 2013] is an alternative widely used in real-time rendering. The specular term is approximated as

$$c_{\text{specular}} \approx L_{\text{specular}} \cdot ((1 - \mathbf{m}) \times 0.04 + \mathbf{m} \times \mathbf{a}) \times F_1 + F_2, \quad (8)$$

where F_1, F_2 are two scalars from a pre-computed table. The diffuse term is computed as

$$c_{\text{diffuse}} = \frac{\mathbf{a}(1 - \mathbf{m})}{\pi} \cdot L_{\text{diffuse}}. \quad (9)$$

L_{diffuse} and L_{specular} can be directed queried for a pre-filtered environment map or neural light representations. The rendered color $c(\omega_o)$ is computed as $c(\omega_o) = c_{\text{diffuse}} + c_{\text{specular}}$.

However, as illustrated in the main paper, when the roughness is very small, the split-sum approximation leads to blurry results. We render a mirror-like plane in Blender using Cycle path-tracing renderer and in the DiffRast [Laine et al. 2020] using the split-sum approximation. The comparison is in Fig. 1, and we can see the split-sum result is blurry.

3 LIGHT MODELING

Considering the efficiency of the light query, we use a simple differential environment map and do not model the indirect illumination and occlusion. The environment light is in the cube map format, whose resolution is $6 \times 512 \times 512$.

4 MORE RESULTS

In this section, we present more results and comparisons.

4.1 Glossy Blender Dataset

We present the LPIPS [Zhang et al. 2018] of relighting images on the Glossy Blender dataset in Tab. 1 and Tab. 2. Our method outperforms Gaussian-based methods along with some NeRF-based ones and is competitive with the current SOTA method.

4.2 Shiny Blender dataset

We show the NVS and relighting results on the Shiny Blender dataset [Verbin et al. 2022]. The quantitative comparison of NVS results are in Tab. 3 and Tab. 4. Our method outperforms the existing Gaussian-based methods on most scenes. However, our method fails in the “coffee” scene, for the deferred pipeline assumes an opaque surface, and the liquid in the “coffee” does not meet the assumption. As illustrated in Fig. 3, our method can provide sharper highlights and more realistic NVS results. We present the relighting result in Fig. 4. Our method provides photo-realistic relighting results, while other Gaussian-based methods fail to render highlights under novel light conditions. We show decomposed maps in Fig. 5, and our method can provide reasonable BRDF decomposition. Besides, we present a comparison of normal estimation in Fig. 6. Thanks to the SDF priors, our method can provide robust normal estimation, while the results of other Gaussian-based methods are overfitted or noisy.

4.3 TensorIR synthetic dataset

We present the relighting quality of Gaussian-based methods on the TensorIR synthetic dataset [Jin et al. 2023] in terms of LPIPS in Tab. 5 and the relighting visualization in Fig. 7. The relighting comparison with NeRF-based methods is in terms of PSNR, SSIM in Tab. 6 and LPIPS in Tab. 7. And the relighting visualization of NeRF-based methods is in Fig. 8. We also show the decomposed maps in

Table 1. Relighting quality with Gaussian-based methods on the Glossy Blender dataset in terms of LPIPS↓.

	GS-IR	RelightGS	GShader	Ours
Angel	0.1901	0.1428	<u>0.1181</u>	0.0858
Bell	0.5203	0.1431	<u>0.1329</u>	0.0795
Cat	0.1591	0.1171	<u>0.1114</u>	0.0596
Horse	0.1606	0.0866	<u>0.0498</u>	0.0356
Luyu	0.1391	0.1094	<u>0.1057</u>	0.0672
Potion	0.2142	0.1614	<u>0.1832</u>	0.0937
Tbell	0.3368	0.1970	<u>0.1877</u>	0.0953
Teapot	0.1716	0.1312	<u>0.1194</u>	0.0982
Mean	0.2365	0.1361	<u>0.1260</u>	0.0769

Table 2. Relighting quality with NeRF-based methods on the Glossy Blender dataset in terms of LPIPS↓.

	TensorIR	MII	TensoSDF	NeRO	Ours
Angel	0.2739	0.1404	<u>0.0871</u>	0.1923	0.0858
Bell	0.2806	0.1534	<u>0.0263</u>	0.0189	0.0795
Cat	0.2146	0.1429	0.0675	0.0455	<u>0.0596</u>
Horse	0.2913	0.0713	0.0318	0.0410	<u>0.0356</u>
Luyu	0.2463	0.1393	0.0807	<u>0.0696</u>	0.0672
Potion	0.2954	0.1747	<u>0.0759</u>	0.0623	0.0937
Tbell	0.2786	0.1938	<u>0.0543</u>	0.0407	0.0953
Teapot	0.2030	0.1426	<u>0.0485</u>	0.0193	0.0982
Mean	0.2605	0.1448	<u>0.0590</u>	0.0612	0.0769

Fig. 9, and the comparison of normal with Gaussian-based methods in Fig. 10. These results of diffuse objects reveal that though our design focuses on reflective surfaces, it can benefit diffuse objects.

Table 3. NVS quality with Gaussian-based methods on Shiny Blender dataset in terms of PSNR↑ and SSIM↑.

	GS-IR	RelightGS	GShader	Ours
Ball	18.30/.7584	21.39/.9047	<u>30.40/.9623</u>	35.50/.9849
Car	25.30/.8867	26.59/.9267	<u>28.39/.9388</u>	30.52/.9638
Coffee	30.72/.9463	32.57/.9710	<u>30.79/.9690</u>	29.64/.9568
Helmet	25.08/.9018	26.95/.9469	<u>28.78/.9549</u>	32.62/.9738
Teapot	38.21/.9900	<u>43.86/.9963</u>	43.35/.9957	43.88/.9964
Toaster	18.66/.7418	20.07/.8745	<u>23.95/.9130</u>	25.89/.9379
Mean	26.05/.8708	28.57/.9367	<u>30.94/.9556</u>	33.01/.9689

Table 4. NVS quality with Gaussian-based methods on Shiny Blender dataset in terms of LPIPS↓.

	GS-IR	RelightGS	GShader	Ours
Ball	0.2966	0.2169	<u>0.1358</u>	0.0842
Car	0.0849	0.0533	<u>0.0477</u>	0.0330
Coffee	0.1125	0.0841	<u>0.0853</u>	0.1035
Helmet	0.1618	0.1014	<u>0.0866</u>	0.0482
Teapot	0.0222	0.0097	<u>0.0108</u>	0.0079
Toaster	0.2479	0.1523	<u>0.1017</u>	0.0859
Mean	0.1543	0.1030	<u>0.0779</u>	0.0605

Table 5. Relighting quality with Gaussian-based methods on the TensorIR synthetic dataset in terms of LPIPS↓.

	GS-IR	RelightGS	GShader	Ours
Armad.	0.0821	<u>0.0593</u>	0.0649	0.0482
Ficus	0.0956	0.0366	0.0437	<u>0.0439</u>
Hotdog	0.1408	<u>0.0880</u>	0.1275	0.0771
Lego	0.1193	<u>0.0902</u>	0.1423	0.0724
Mean	0.1095	<u>0.0685</u>	0.0946	0.0604

Table 6. Relighting quality with NeRF-based methods on the TensorIR synthetic dataset in terms of PSNR↑ and SSIM↑.

	MII	NeRO	TensoSDF	TensorIR	Ours
Armad.	26.85/.9441	23.02/.9335	23.02/.9355	34.51/.9754	<u>31.33/.9593</u>
Ficus	20.65/.9068	<u>27.43/.9404</u>	28.53/.9499	24.32/.9465	26.28/.9542
Hotdog	22.65/.9011	20.45/.9262	20.47/.9241	27.92/.9324	<u>25.21/.9307</u>
Lego	23.20/.8643	17.76/.8577	17.92/.8670	27.61/.9253	<u>25.46/.9083</u>
Mean	23.34/.9041	22.17/.9145	22.48/.9191	28.59/.9449	<u>27.07/.9381</u>

Table 7. Relighting quality with NeRF-based methods on the TensorIR synthetic dataset in terms of LPIPS↓.

	MII	NeRO	TensoSDF	TensoIR	Ours
Armad.	0.0692	0.0644	0.0578	0.0368	<u>0.0483</u>
Ficus	0.0728	0.0677	<u>0.0533</u>	0.0543	0.0439
Hotdog	0.0893	0.0888	<u>0.0906</u>	0.0833	0.0771
Lego	0.1715	0.1228	0.1088	0.0702	<u>0.0723</u>
Mean	0.1007	0.0859	0.0776	<u>0.0612</u>	0.0604

REFERENCES

- Brent Burley and Walt Disney Animation Studios. 2012. Physically-based shading at disney. In *SIGGRAPH*.
- Yingwenqi Jiang, Jiadong Tu, Yuan Liu, Xifeng Gao, Xiaoxiao Long, Wenping Wang, and Yuexin Ma. 2024. GaussianShader: 3D Gaussian Splatting with Shading Functions for Reflective Surfaces. In *CVPR*.
- Haian Jin, Isabella Liu, Peijia Xu, Xiaoshuai Zhang, Songfang Han, Sai Bi, Xiaowei Zhou, Zexiang Xu, and Hao Su. 2023. TensorIR: Tensorial Inverse Rendering. In *CVPR*.
- Brian Karis and Epic Games. 2013. Real shading in unreal engine 4. *Proc. Physically Based Shading Theory Practice* (2013).
- Bernhard Kerbl, Georgios Kopanas, Thomas Leimkühler, and George Drettakis. 2023. 3D Gaussian Splatting for Real-Time Radiance Field Rendering. *ACM TOG* (2023).
- Samuli Laine, Janne Hellsten, Tero Karras, Yeongho Seol, Jaakko Lehtinen, and Timo Aila. 2020. Modular Primitives for High-Performance Differentiable Rendering. *ACM TOG* (2020).
- Dor Verbin, Peter Hedman, Ben Mildenhall, Todd Zickler, Jonathan T. Barron, and Pratul P. Srinivasan. 2022. Ref-NeRF: Structured View-Dependent Appearance for Neural Radiance Fields. In *CVPR*.
- Richard Zhang, Phillip Isola, Alexei A Efros, Eli Shechtman, and Oliver Wang. 2018. The unreasonable effectiveness of deep features as a perceptual metric. In *CVPR*.



Fig. 2. NVS results on the Glossy dataset. Our method provides photo-realistic NVS results for reflective objects, while other Gaussian-based methods fail.

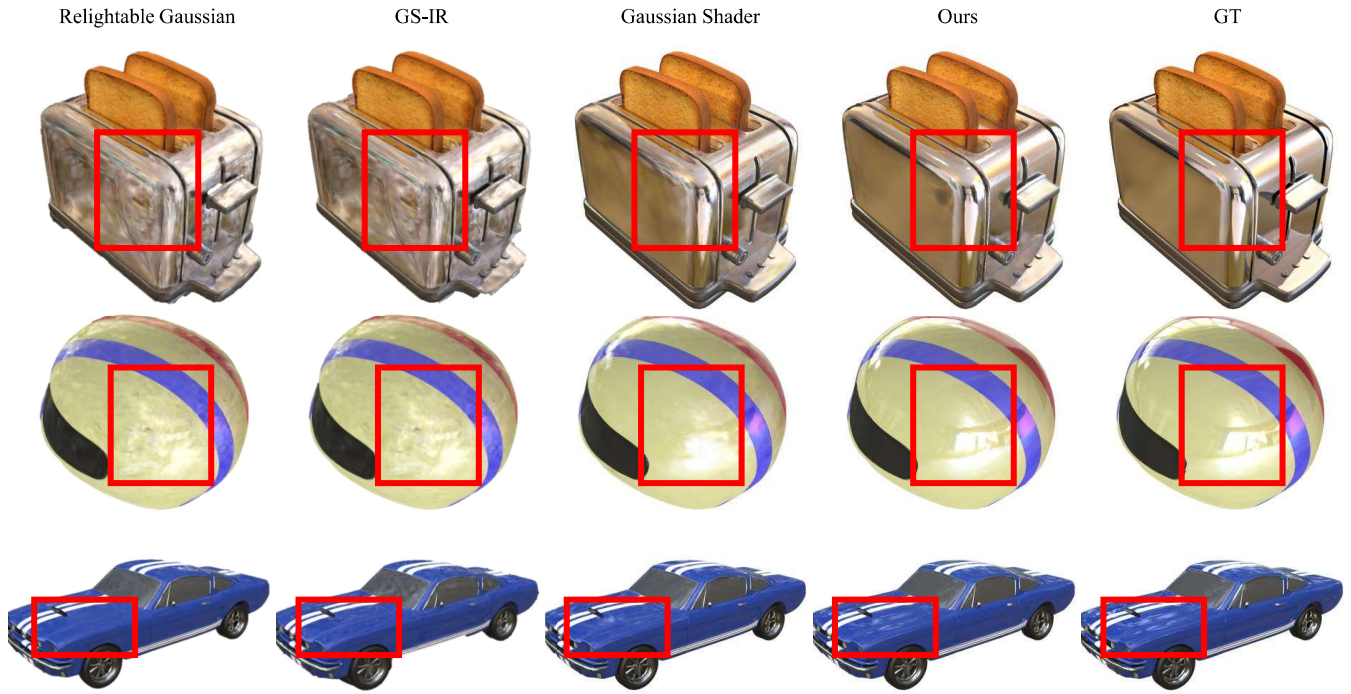


Fig. 3. NVS results of Gaussian-based methods on the Shiny Blender dataset. Our method preserves correct highlights, while others fail to render sharp highlights.

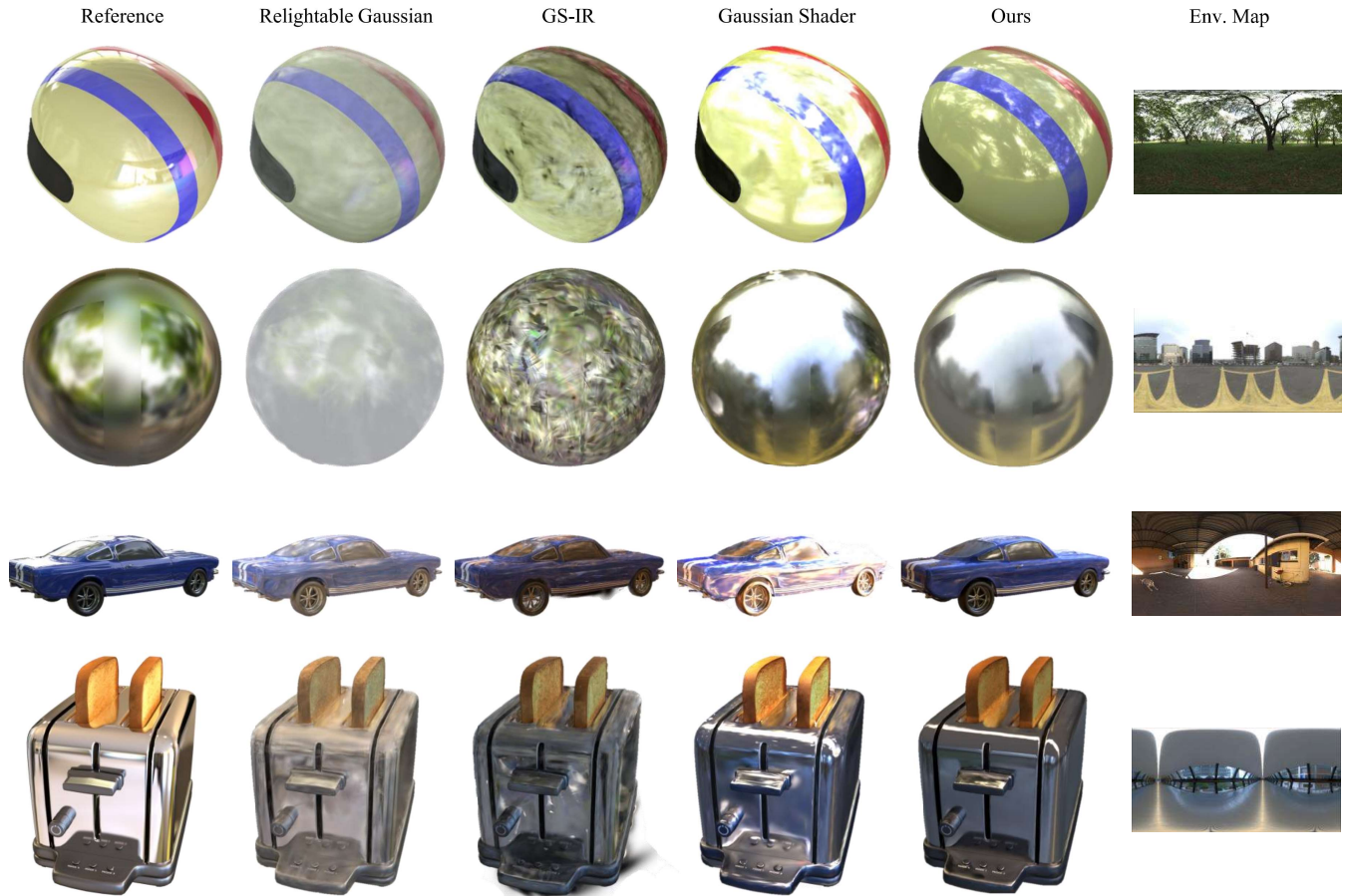


Fig. 4. Relighting results of Gaussian-based methods on the Shiny Blender dataset. Note that no relighting ground truth is available, so we only show the relighting examples. Our method can provide reasonable relighting results under diverse lighting conditions.

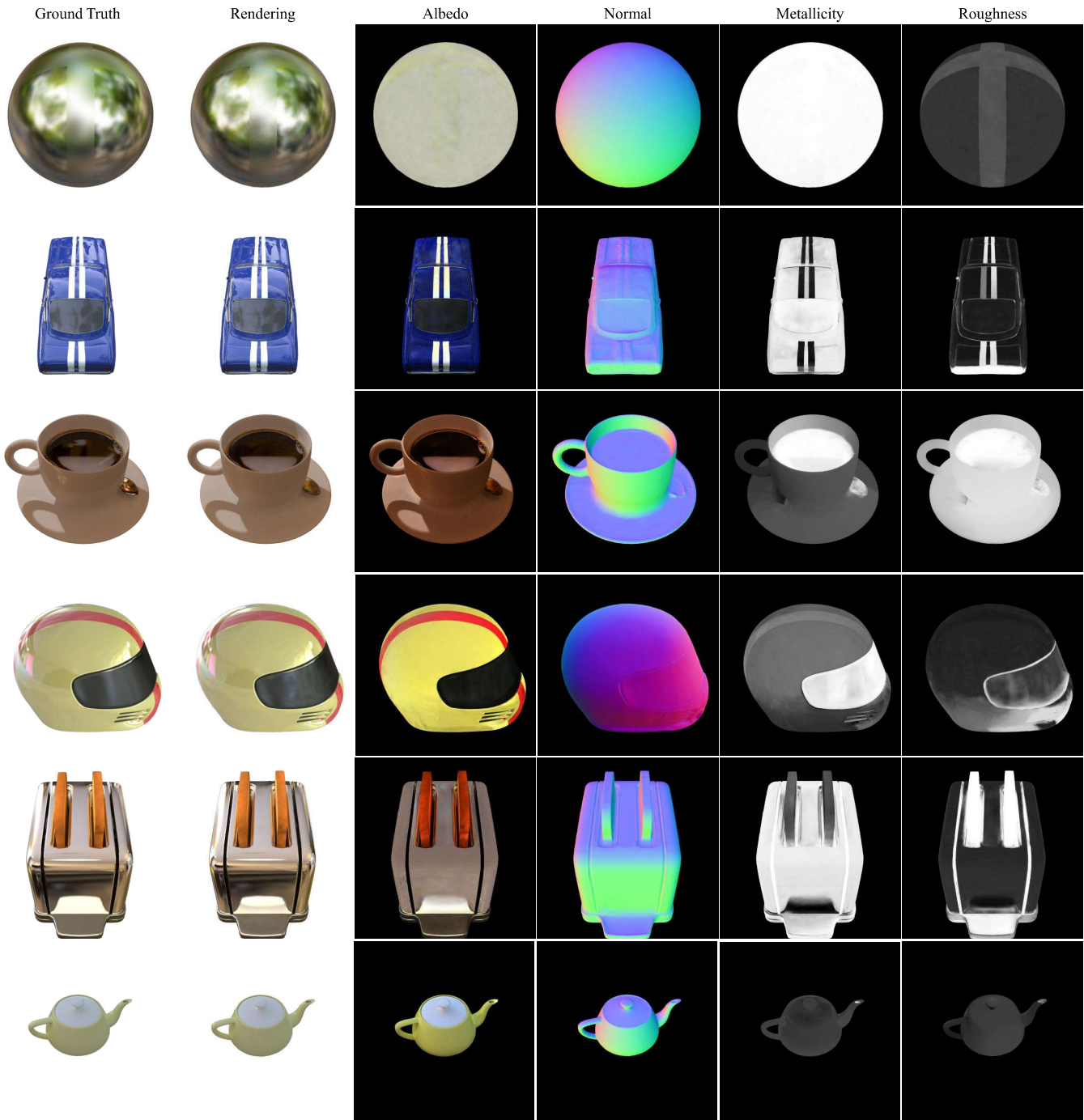


Fig. 5. Normal and BRDF decomposed maps on the Shiny Blender dataset. Our method provides robust normal estimation and reasonable BRDF decomposition.

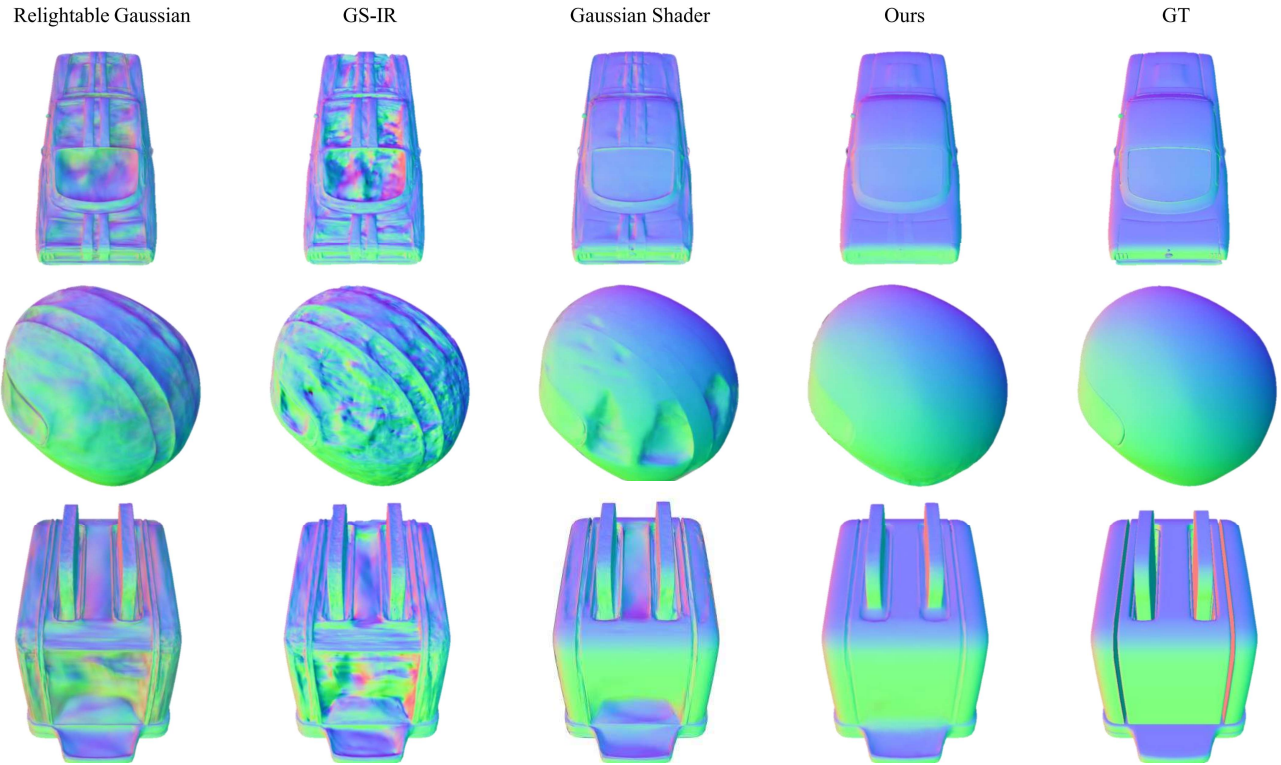


Fig. 6. Normal comparison with Gaussian-based methods on the Shiny Blender dataset. Our method provides robust normal estimation, while other results are noisy or overfitted.



Fig. 7. Relighting results of Gaussian-based methods on the TensoIR synthetic dataset. Our method can also provide high-quality relighting results for diffuse objects and outperforms the existing Gaussian-based methods.



Fig. 8. Relighting results of NeRF-based methods on the TensoIR synthetic dataset. Our method can also provide high-quality relighting results for diffuse objects and outperforms most NeRF-based methods.

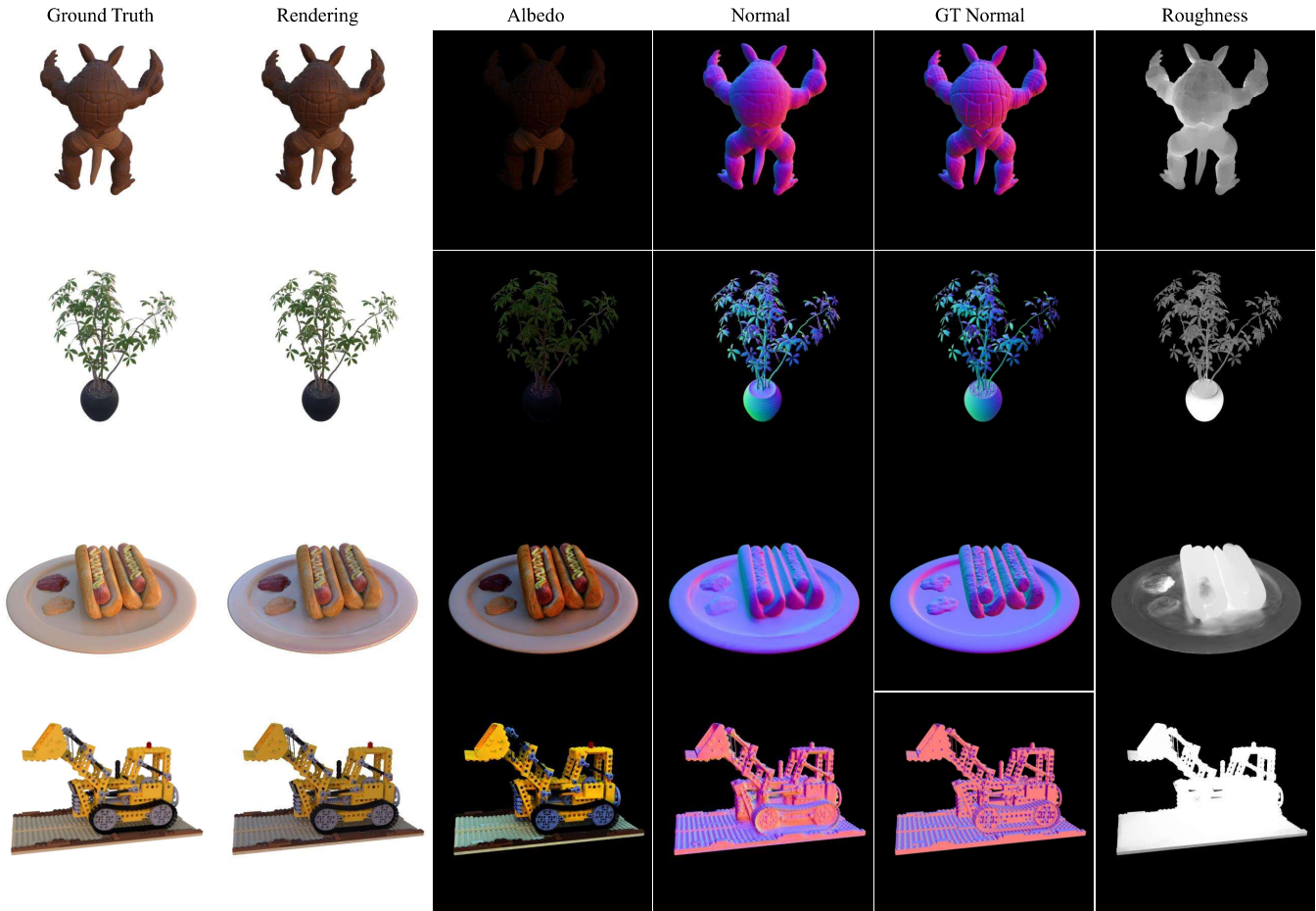


Fig. 9. Normal and BRDF decomposed maps of our method on the TensoIR synthetic dataset. Our method can also provide reasonable BRDF estimation for diffuse objects.

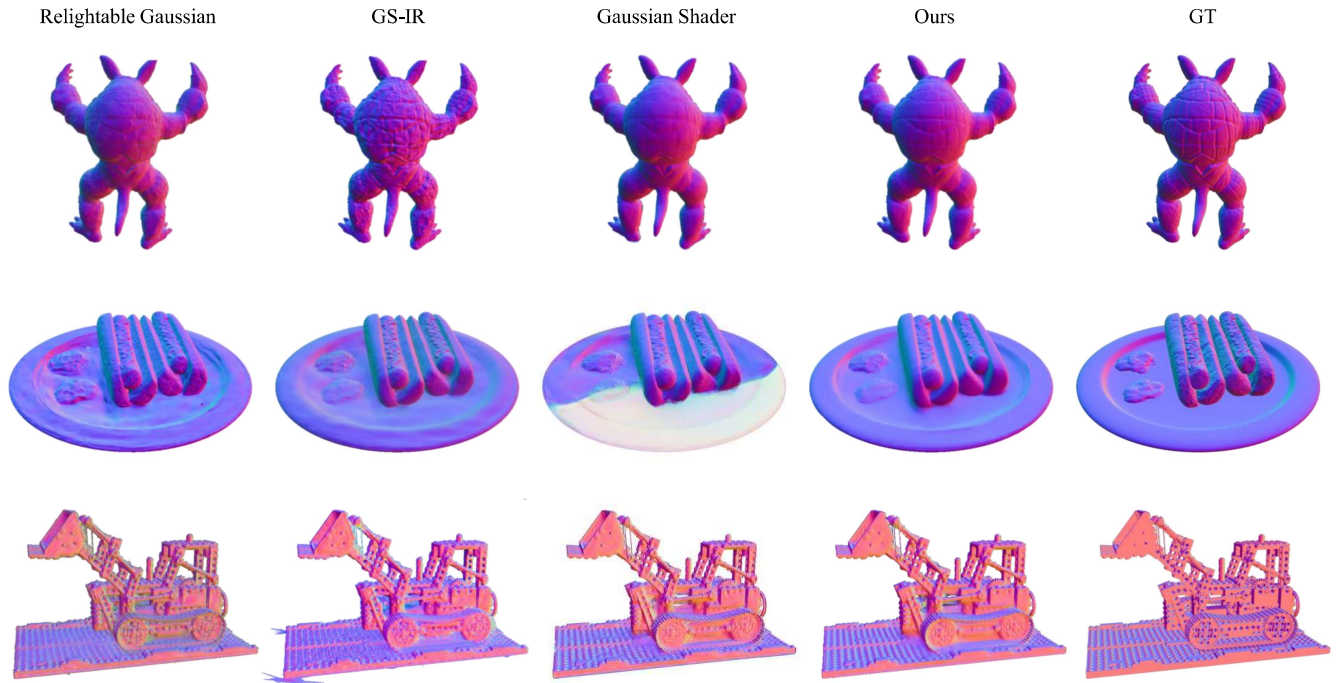


Fig. 10. Normal comparison with Gaussian-based methods on the TensorR synthetic dataset. Our method can also provide robust normal estimation for diffuse objects.

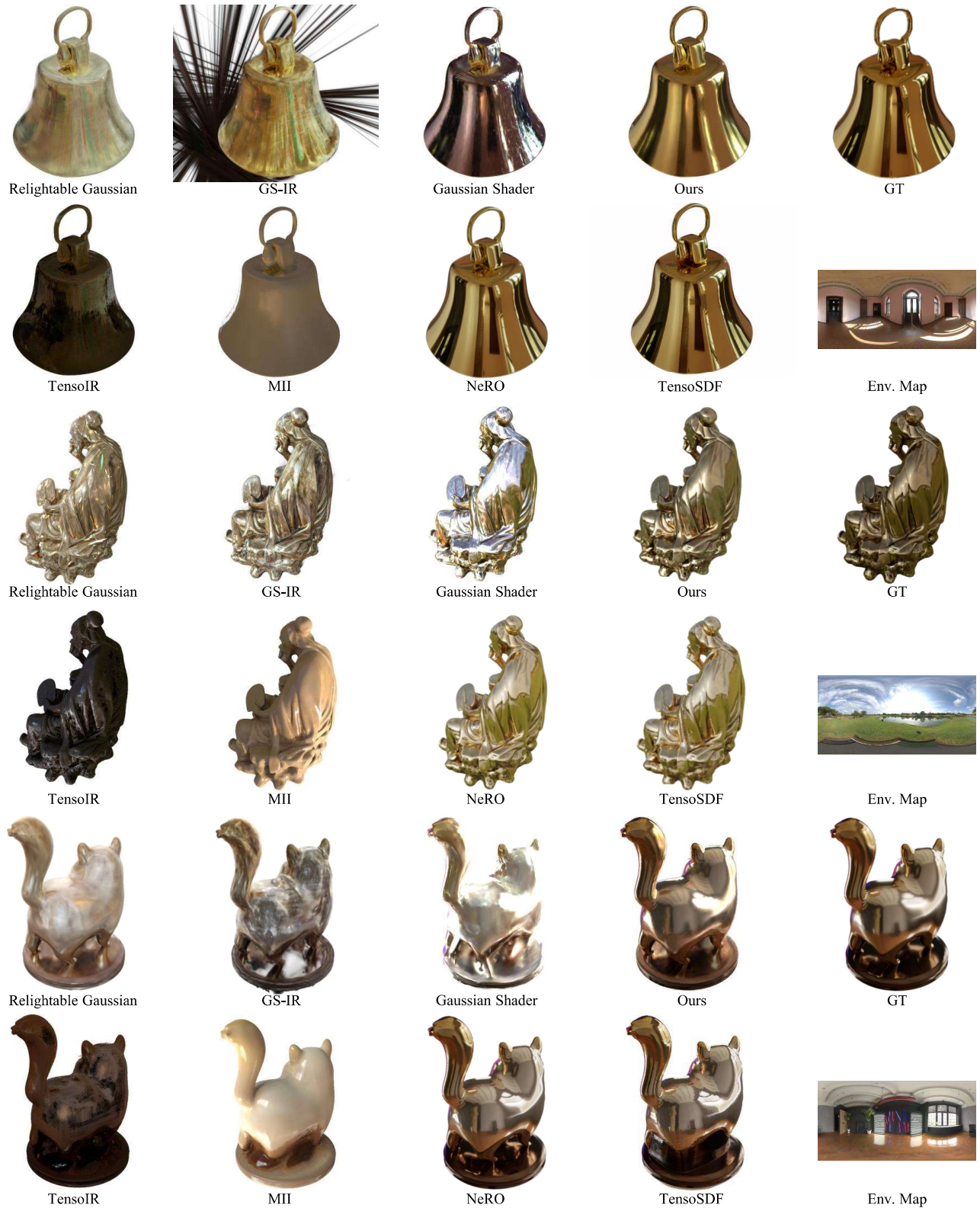


Fig. 7. Relighting results on the Glossy Blender Dataset. Relightable Gaussian, GS-IR, TensoIR, and MII fail to model specular highlights. Gaussian Shader provides specular relighting results with obvious artifacts. Our method, along with NeRO and TensoSDF, provides high-quality results, while our method only uses 25% training time of TensoSDF and enables real-time relighting.

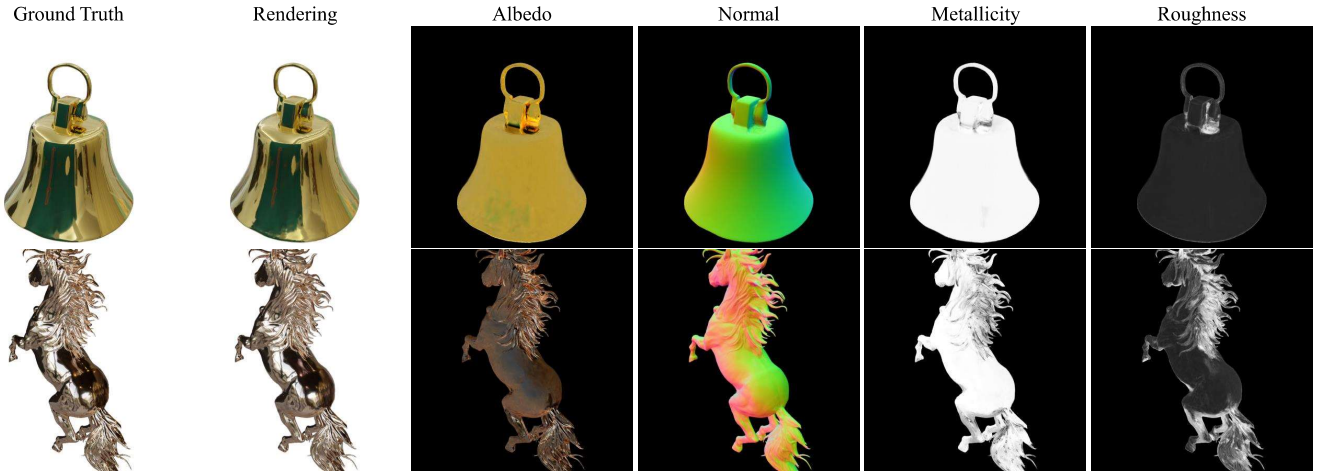


Fig. 8. Decomposed maps of our method on the Glossy Blender Dataset. Our method can provide a reasonable decomposition for reflective surfaces. The normal is smooth but also maintains details (see the horse mane in the 2nd row).

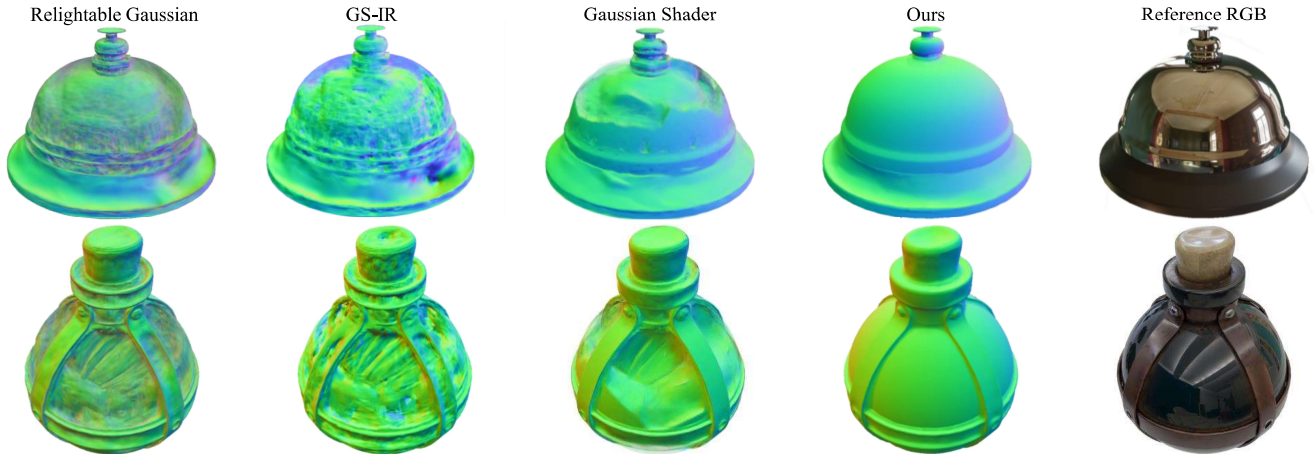


Fig. 9. Normal comparison among Gaussian-based methods on the Glossy Blender Dataset. Our method can reconstruct high-quality normal for relighting, while others overfit under the training scene and provide erroneous normal.



Fig. 10. Relighting results on real data from NeLF++. Relightable Gaussian and GS-IR fail to reconstruct the reflective objects in real scenes. Gaussian Shader cannot relight the specular highlights faithfully, while our method can provide reasonable relighting results.